2012

Predicting impacts of increased CO2 and climate change on the water cycle and water quality in the semiarid James River Basin of the Midwestern USA

Yiping Wu
U.S. Geological Survey (USGS) Earth Resources Observation and Science (EROS) Center, ywu@usgs.gov

Shuguang Liu
U.S. Geological Survey, sliu@usgs.gov

Alisa L. Gallant
U.S. Geological Survey (USGS) Earth Resources Observation and Science (EROS) Center, gallant@usgs.gov

Science of the Total Environment 430 (2012) 150–160

Contents lists available at SciVerse ScienceDirect

Science of the Total Environment

journal homepage: www.elsevier.com/locate/scitotenv

Predicting impacts of increased CO_2 and climate change on the water cycle and water quality in the semiarid James River Basin of the Midwestern USA

Yiping Wu [a], Shuguang Liu [b,c,*], Alisa L. Gallant [b,c]

[a] ASRC Research and Technology Solutions, contractor to the U.S. Geological Survey (USGS) Earth Resources Observation and Science (EROS) Center, Sioux Falls, SD 57198, United States
[b] U.S. Geological Survey (USGS) Earth Resources Observation and Science (EROS) Center, Sioux Falls, SD 57198, United States
[c] Geographic Information Science Center of Excellence, South Dakota State University, Brookings, SD 57007, United States

ARTICLE INFO

Article history:
Received 2 March 2012
Received in revised form 23 April 2012
Accepted 23 April 2012
Available online 26 May 2012

Keywords:
CO_2
Groundwater recharge
Nitrate nitrogen
Soil water content
SWAT

ABSTRACT

Emissions of greenhouse gases and aerosols from human activities continue to alter the climate and likely will have significant impacts on the terrestrial hydrological cycle and water quality, especially in arid and semiarid regions. We applied an improved Soil and Water Assessment Tool (SWAT) to evaluate impacts of increased atmospheric CO_2 concentration and potential climate change on the water cycle and nitrogen loads in the semiarid James River Basin (JRB) in the Midwestern United States. We assessed responses of water yield, soil water content, groundwater recharge, and nitrate nitrogen (NO_3–N) load under hypothetical climate-sensitivity scenarios in terms of CO_2, precipitation, and air temperature. We extended our predictions of the dynamics of these hydrological variables into the mid-21st century with downscaled climate projections integrated across output from six General Circulation Models. Our simulation results compared against the baseline period 1980 to 2009 suggest the JRB hydrological system is highly responsive to rising levels of CO_2 concentration and potential climate change. Under our scenarios, substantial decrease in precipitation and increase in air temperature by the mid-21st century could result in significant reduction in water yield, soil water content, and groundwater recharge. Our model also estimated decreased NO_3–N load to streams, which could be beneficial, but a concomitant increase in NO_3–N concentration due to a decrease in streamflow likely would degrade stream water and threaten aquatic ecosystems. These results highlight possible risks of drought, water supply shortage, and water quality degradation in this basin.

Published by Elsevier B.V.

1. Introduction

Climate change occurs naturally, but human population growth and associated land-cover conversion (e.g., deforestation) and burning of fossil fuel have substantially accelerated the increase of greenhouse gases (CO_2, CH_4, N_2O, etc.). Elevated concentrations of CO_2 and other greenhouse gases from anthropogenic activities have caused warming of the global climate by modifying radiative forcings, and continued changes likely will result in climate shifts (Houghton et al., 2001; Stone et al., 2001).

Elevated atmospheric CO_2 concentration directly affects plant growth, which inherently is tied with the hydrological cycle (Eckhardt and Ulbrich, 2003; Ficklin et al., 2009), through lowered rates of stomatal conductance and increases in leaf area (Field et al., 1995; Medlyn et al., 2001; Morison, 1987; Saxe et al., 1998; Wand et al., 1999). Decreased stomatal conductance could reduce evapotranspiration (ET) (Stockle et al., 1992b), whereas increased leaf area could contribute to increases in ET (Kergoat et al., 2002; Pritchard et al., 1999), potentially offsetting the reduction in stomatal conductance to some degree (Betts et al., 1997; Kergoat et al., 2002). Many studies have indicated that combined effects from elevated CO_2 concentrations may lessen ET, resulting in increased runoff (Betts et al., 2007; Eckhardt and Ulbrich, 2003; Gedney et al., 2006; Leipprand and Gerten, 2006). However, global warming can increase the ability of air to absorb water as temperatures rise, suggesting increases in potential evapotranspiration (PET) (Jha et al., 2006).

A further consequence of elevated concentrations of greenhouse gases may be changes in spatiotemporal distribution and magnitude of precipitation (Bates et al., 2008; Eckhardt and Ulbrich, 2003; Houghton et al., 2001; Labat et al., 2004; Zhou et al., 2011). For example, Labat et al. (2004) identified a link between global warming and intensification of the hydrological cycle at the global scale using a statistical wavelet-based method; although, there has been disagreement on the strength

* Corresponding author at: U.S. Geological Survey (USGS) Earth Resources Observation and Science (EROS) Center, Sioux Falls, SD 57198, United States. Tel.: +1 605 594 6168; fax: +1 605 594 6529.
E-mail addresses: ywu@usgs.gov (Y. Wu), sliu@usgs.gov (S. Liu), gallant@usgs.gov (A.L. Gallant).

0048-9697/$ – see front matter. Published by Elsevier B.V.
doi:10.1016/j.scitotenv.2012.04.058

of the evidence (Labat et al., 2005; Legates et al., 2005). However, such intensification has been demonstrated through long-term observations in an intact forested watershed in Southern China (Zhou et al., 2011), which exhibited intensified rainfall and a rise in the water table despite more annual days without rain, no gain in soil moisture, and no clear change in annual total rainfall. This shift in climatic characteristics simultaneously exacerbated flooding (from intensified rainfall) and drought (from substantial decrease in soil moisture) (Zhou et al., 2011).

Many studies based on observations and modeling have implied increased CO_2 concentrations and climate change have significant impacts on hydrological systems (Gedney et al., 2006; Jackson et al., 2001; Jha et al., 2006; Koster et al., 2004; Labat et al., 2004; Piao et al., 2009; Schaake, 1990; Wu et al., 2012; Zhou et al., 2011). These potential impacts can be quantified for a specific watershed using hydrological models with hypothetical climate-sensitivity scenarios or future climate projections derived from General Circulation Models (GCMs). This proactive approach highlights environmental concerns of interest for resource management and policy decisions. For example, the physically-based Soil and Water Assessment Tool (SWAT) (Arnold et al., 1998; Neitsch et al., 2005) has been widely used for evaluating climate-change effects on hydrological processes and nonpoint source pollution at watershed scales (Chaplot, 2007; Ficklin et al., 2010, 2009; Fontaine et al., 2001; Jha et al., 2006; Vicuna et al., 2007; Wilson and Weng, 2011; Xu et al., 2009; Young et al., 2009). Wu et al. (2012) modified SWAT (version 2005) to improve representation of more mechanistic vegetation type responses (stomatal conductance reduction and leaf area increase) to elevated CO_2 concentrations. For the current study, we used this modified version of SWAT to assess climate-change effects on the water cycle and nitrate nitrogen (NO_3–N) loads in the James River Basin (JRB), a large semiarid basin in the midwestern United States. We quantified the sensitivity of hydrological/water quality responses to climate change with a group of climate-sensitivity scenarios including CO_2, precipitation, and air temperature changes. We then assessed potential impacts of climates with downscaled and debiased climate projections integrated across output from six GCMs under three different scenarios of greenhouse gas emissions by the mid-21st century.

2. Materials and methods

2.1. Study area

The James River is a tributary of the Missouri River in the United States. This river begins in North Dakota and runs south into South Dakota before intersecting with the Missouri River. The streamflow and water quality gage (USGS gage number: 6478500) near Scotland, South Dakota, is located close to the mouth of the James River, monitoring a drainage area of about 53,490 km^2 (Fig. 1). The JRB is part of the semiarid Northern Great Plains in the United States and receives an average of 528 mm of precipitation annually based on the 49-year (1961–2009) precipitation data available for this basin (http://www.ncdc.noaa.gov). The average annual discharge near Scotland is 24 m^3/s, according to streamflow gaging data for the same period (http://waterdata.usgs.gov/nwis/sw).

2.2. SWAT and its modification

The SWAT model was developed by the U.S. Department of Agriculture (USDA) Agricultural Research Service (Arnold et al., 1998), for exploring the effects of climate and land management practices on water, sediment, and agricultural chemical yields. This physically-based watershed model simulates the hydrological cycle, cycles of plant growth, transportation of sediment, and agricultural chemical yields on a daily time step (Arnold et al., 1998). The hydrological part of the model is based on the water-balance equation in the soil profile, with terms representing processes of precipitation, surface runoff, infiltration, evapotranspiration, lateral flow, percolation, and groundwater flow (Arnold et al., 1998; Neitsch et al., 2005). We selected the Penman–Monteith method to estimate PET for this study.

SWAT incorporates the Erosion Productivity Impact Calculator (EPIC) (Sharpley and Williams, 1990; Williams, 1995) for simulating crop growth that influences the hydrological cycle. Thus, impacts of vapor pressure deficit and radiation-use efficiency on leaf conductance and plant growth (Stockle et al., 1992a, 1992b) are addressed in SWAT (Neitsch et al., 2005). In a previous study (Wu et al., 2012), we improved the SWAT model (version 2005) by representing vegetation type specific responses (stomatal conductance reduction and leaf area increase) to elevated atmospheric CO_2 concentrations with information from a number of physiological studies. For major land-cover types such as cropland, forest (mixed), and grassland, the percent change for conductance reduction under a doubling of CO_2 concentration (i.e., from 330 ppm to 660 ppm) is 40%, 16%, and 26%, respectively; and the percentage for leaf area increase is 37%, 7%, and 20%, respectively. This percent change is assumed to be linear over the entire range of CO_2 concentrations between 330 ppm and 660 ppm (Morison and Gifford, 1983). Further details about model modification have been described in Wu et al. (2012). We also incorporated long-term (1960–2009) observed CO_2 concentrations into the model to help detect the historical impacts of the increased CO_2 in past decades (Wu et al., 2012). We applied this modified version of SWAT for the current study to represent more accurately the effects of elevated CO_2 concentrations on the hydrological cycle in the JRB.

2.3. Model input and setup

We used ArcSWAT (Winchell et al., 2009), a Geographic Information System interface, to automate development of model input parameters. We obtained elevation data from the National Elevation Dataset (http://ned.usgs.gov) and resampled the cell resolution from the native 10 m to 90 m for deriving subbasins. This discretization resulted in 83 subbasins for the JRB. We combined information from the 30-m 2001 National Land Cover Database (Homer et al., 2007) for non-agricultural areas with the 56-m USDA National Agricultural Statistics Service (NASS) cropland data layer (Craig, 2010) for agricultural areas as land-cover input for model parameterization. We applied the multiple Hydrological Response Unit (HRU) model option in SWAT to represent land uses and soil types as separate HRUs within a subbasin, resulting in discretization of 1144 HRUs for the JRB. We obtained daily precipitation and air temperature data from the National Climatic Data Center (http://www.ncdc.noaa.gov) and generated daily values for solar radiation, wind speed, and relative humidity with the SWAT model weather generator using the multiyear average monthly statistics provided within the SWAT database.

We examined four years of NASS cropland maps (2006–2009) to identify the dominant crop rotations occurring on agricultural lands in the basin. We used the multiyear (1991–2007) average nitrogen fertilizer application rate of 109 kg N/ha (98 lb/ac) (http://www.ers.usda.gov/Data/FertilizerUse) to parameterize the model. We consulted the literature (Jha et al., 2010; Thomas et al., 2009) for planting and harvesting dates for corn and soybean, the most widespread row crops in the JRB. We omitted irrigation practices in the model because the irrigated area only accounts for less than 1% of the basin area (Pervez and Brown, 2010; USGS, 2002).

2.4. Model calibration and validation

Many hydrological models contain parameters that cannot be determined from field measurements directly (Beven, 2001). Therefore, model calibration is used to adjust such parameters to optimize the agreement between observations and simulations

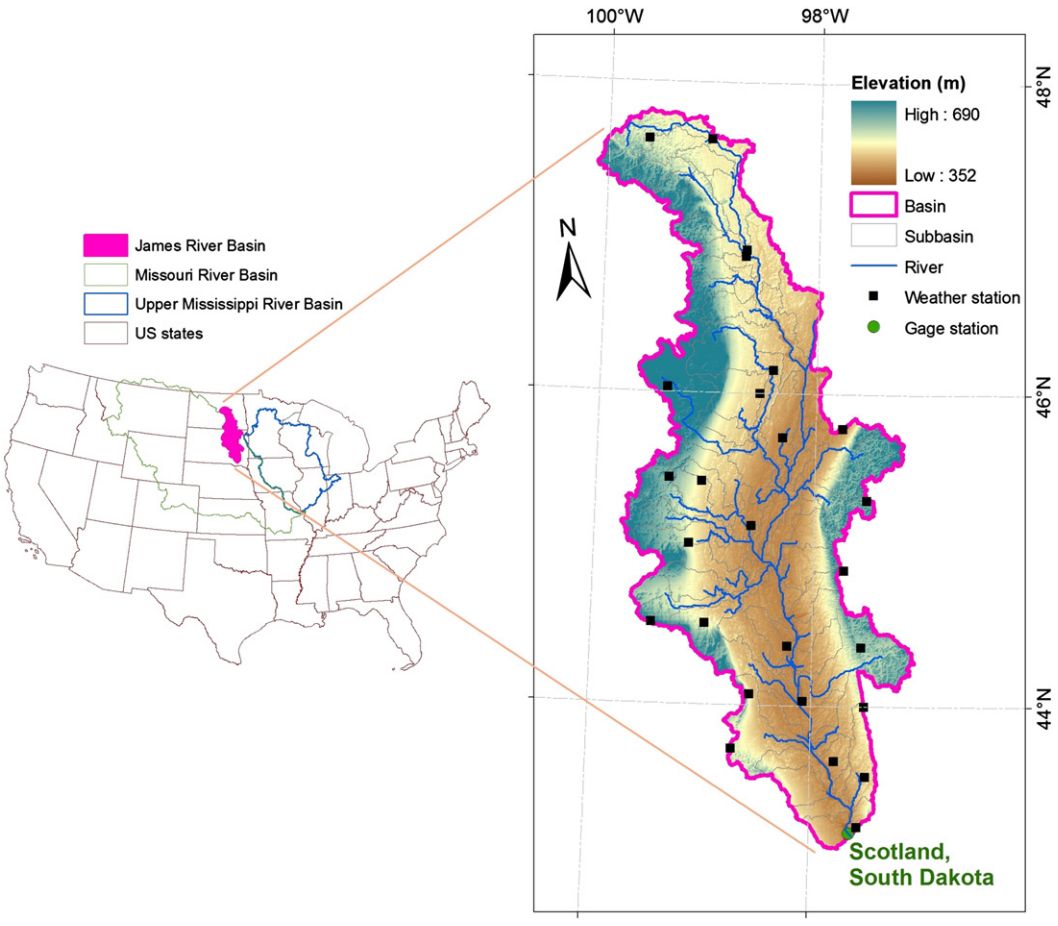

Fig. 1. Location of the James River Basin.

(Tolson and Shoemaker, 2007; Zhang et al., 2009). We calibrated the SWAT model with ten-year (1991–2000) records of monthly streamflow and NO_3–N load collected from the gage near Scotland (Fig. 1), then validated output with data collected for the subsequent nine years (2001–2009). A three–year (1988–1990) warm-up period was used to minimize the impacts of uncertain initial conditions (e.g., soil water storage) in the model simulation. The model also was validated with data for the 30-year timeframe of 1980–2009, which was the baseline period for assessing climate-change impacts in the basin (see Section 2.5).

We selected eight parameters for model calibration in this basin based on the literature review related to SWAT model calibration (Arabi et al., 2008; Muleta and Nicklow, 2005; Santhi et al., 2001) (Table 1). The parameter sensitivity analysis showed CN2, ALPHA_BF, SURLAG, and ESCO are the most sensitive parameters. We then used the auto-calibration procedure (Green and van Griensven, 2008; van Griensven et al., 2006), which incorporates the Shuffled Complex Evolution algorithm developed by the University of Arizona (SCE-UA) (Duan et al., 1992) to optimize the parameters across the basin until an acceptable fit was obtained between the observation and simulation. The criteria we used to assess model performance included Percentage Bias (PB), Nash–Sutcliffe Efficiency (NSE) (Nash and Sutcliffe, 1970), and R^2, and the corresponding equations can be found in Appendix A.

2.5. Climate-sensitivity scenarios

A sensitivity analysis can provide valuable insights into the magnitude of responses of hydrological systems to various components of climate change (Arnell and Liv, 2001). This approach generally relies on a baseline scenario to reflect current conditions. We used climate data for the past 30 years (1980–2009) to define baseline conditions under an average atmospheric CO_2 concentration of 361 ppm (NOAA/ESRL, 2010) for the timeframe. We designed a sensitivity analysis to assess hydrological responses to changing levels of CO_2, precipitation, and air temperature, altering the level of one variable while holding the others constant (see Table 2). A doubled CO_2 concentration (i.e., 722 ppm) is expected by the end of the 21st century under the A1B greenhouse gas emission scenario (IPCC, 2001). We ran nine sensitivity scenarios in addition to the baseline scenario for the 30-year timeframe.

Table 1
Calibrated parameter values for the James River Basin.

Parameter	Description	Range	Calibrated value/change
CN2	SCS curve number for moisture condition II	−15%–+15%	−14%[a]
SURLAG	Surface runoff lag coefficient	0.1–3.0	1.0
ESCO	Soil evaporation compensation factor	0.1–1.0	0.6
EPCO	Plant uptake compensation factor	0.01–1.0	0.433
ALPHA_BF	Baseflow alpha factor (day)	0.001–0.08	0.048
CH_N2	Manning's n for main channel	0.014–0.16	0.15
NPERCO	Nitrogen percolation factor	0.0–1.0	0.301
CMN	Rate factor for humus mineralization of active organic nitrogen	–	0.00003

[a] CN2 changed −14% relative to the default values.

Table 2
Climate-sensitivity scenarios for annual average conditions relative to reference conditions.

Scenario	CO_2 concentration (ppm)	Precipitation change (%)	Temperature increase (°C)
Reference	361	0	0
1	$1.5\times CO_2 = 542$	0	0
2	$2.0\times CO_2 = 722$	0	0
3	361	+10	0
4	361	+20	0
5	361	−10	0
6	361	−20	0
7	361	0	+1
8	361	0	+2
9	361	0	+4

2.6. Downscaling of climate projections

To assess hydrological effects of potential future climate trajectories, we developed a set of gridded map layers for monthly precipitation and air temperatures for 2040–2069 with output from a set of GCMs parameterized to respond to three greenhouse gas emissions scenarios defined by the Intergovernmental Panel on Climate Change (IPCC, 2000, 2006), including B1 (medium-paced technological change, with emphases on environmental sustainability, globalization, low energy use, and high rates of land-use change), A1B (rapid-paced technological change, with emphases on economic growth, globalization, very high energy use, and low rates of land-use change), and A2 (slow-paced technological change, with emphases on economic growth, regional development, high energy use, and medium to high rates of land-use change). Native spatial resolution of GCM output is coarse, so we applied a downscaling program modified from Hay et al. (2011) to generate large-area climate surfaces at 4-km spatial resolution and a monthly time scale. The modified program (also developed by Hay and colleagues) implemented the change-factor approach described in Tabor and Williams (2010), which we calibrated for a baseline period of 1961–1990, the interval recognized by the World Meteorological Organization. The program developed a climatology for the baseline period from twentieth-century output from each GCM. Change factors then were calculated based on comparing a GCM's prediction for a future period with the departure from its prediction for the baseline period. This addressed bias that would be realized comparing a model's output for a future period with actual (observed) baseline data. Resulting change fields were downscaled spatially with bilinear interpolation to fit finer-scaled geospatial patterns of observed data matching the baseline period. This simple downscaling technique can be applied over extensive areas and can perform as well as more sophisticated methods when the goal is to assess changes in mean climate (Fowler et al., 2007); however, a weakness of the technique is the assumption future geospatial patterns of climate surfaces will mimic those of the past. We obtained monthly climate surfaces from the PRISM Climate Group (http://www.prism.oregonstate.edu) and used cell centers to represent "observed" monthly climate patterns for the baseline period. Our resultant dataset of downscaled projections thus matched the spatial resolution (4 km) of the PRISM surfaces.

Our version of the Hay et al. model (2011) provided downscaled output from six GCMs (BCCR-BCM2, CCSM3, CSIRO3.0-Mk, CSIRO-Mk3.5, INM-CM3.0, and MIROC3.2; see http://www.ipcc-data.org/gcm/monthly/SRES_AR4/index.html). We developed a multi-model ensemble averaged across output from all six GCMs. Combining output across multiple GCMs can provide more reliable representation of regional changes and uncertainties than result from single models by reducing the influences of weaknesses or biases inherited from individual models (Gleckler et al., 2008; Lambert and Boer, 2001; Pierce et al., 2009; Tebaldi and Knutti, 2007). We calculated the mean output across models for each monthly time step and 4-km grid cell for each of the three IPCC emissions scenarios.

We extracted the climate projection data from grid cells in which climate gaging stations were located as input to SWAT. For input of atmospheric CO_2 concentrations to SWAT, we used mean values for 2040 to 2069 (494 ppm for the B1 scenario, 551 ppm for the A1B scenario, and 562 ppm for the A2 scenario) derived based on decadal CO_2 concentration (IPCC, 2001).

3. Results

3.1. Model evaluation

The graphical comparisons of monthly and annual simulated streamflow and NO^3–N load against those observed during the 30-year (1980–2009) baseline simulation period, including ten-year (1991–2000) calibration and nine-year (2001–2009) validation, are shown in Fig. 2. The monthly streamflow simulations matched well with the observations, although two peak flows (e.g., 1995 and 1997) were underestimated and two peak flows (e.g., 1991 and 1993) were overestimated during extreme high-water years (Fig. 2a). Results from the statistical evaluation with the three numeric criteria including PB, NSE, and R^2 (Appendix A), are listed in Table 3. The NSEs for monthly streamflow simulation were 0.55, 0.67, and 0.45 for the ten-year calibration, nine-year validation, and 30-year baseline periods, respectively. Model performance was notably better for annual streamflow (0.75 for calibration, 0.79 for validation, and 0.72 for baseline). The model tended to underpredict streamflow for the calibration (PB = −18.4) and validation (PB = −7.4) periods, but performed quite well for the 30-year baseline period (PB = 0.8). For NO^3–N simulation (Fig. 2c,d), NSEs for monthly simulation were 0.60, 0.67, and 0.50 for the calibration, validation, and 30-year baseline periods, respectively, and better for the annual simulations (0.80 for calibration, 0.77 for validation, and 0.70 for baseline). The PB was best for the calibration period for modeling NO^3–N, with weaker performance for the validation periods (PB = 18.9 for validation and PB = 20.8 for baseline). From this set of evaluations we considered overall model performance for streamflow and NO^3–N simulation to be satisfactory for conducting the climate change sensitivity assessment.

3.2. Climate sensitivity

3.2.1. CO_2 concentration

Scenarios 1 and 2 shown in Table 2 indicate increases of 50% and 100% for the atmospheric CO_2 concentration, with no changes in precipitation and air temperature. These two scenarios were simulated using our modified SWAT model (Wu et al., 2012), which incorporated variable stomatal conductance reduction and leaf area increase specific to vegetation type. Fig. 3a–d depicts simulated monthly average water yield, soil water content, groundwater recharge, and NO^3–N load under the baseline conditions and increased CO_2 concentrations. Water yield herein refers to the sum of the three hydrological components—overland surface runoff, subsurface lateral flow, and groundwater baseflow—that contribute to the water production from an HRU. The higher atmospheric CO_2 concentration resulted in higher water yield and soil water content, along with corresponding increases in groundwater recharge and NO^3–N load. The net effect of reduced stomatal conductance and increased leaf area per unit increase of CO_2 reduced ET. As shown in Fig. 3a,c, this kind of vegetation response (evident through increased water yield and groundwater recharge) to elevated CO_2 is more pronounced in the growing season, especially from May to July. Table 4 indicates annual ET will decline by 3% (about 16 mm) under a doubling of atmospheric CO_2 concentration (i.e., 722 ppm), which is expected by the end of the 21st century under the A1B greenhouse

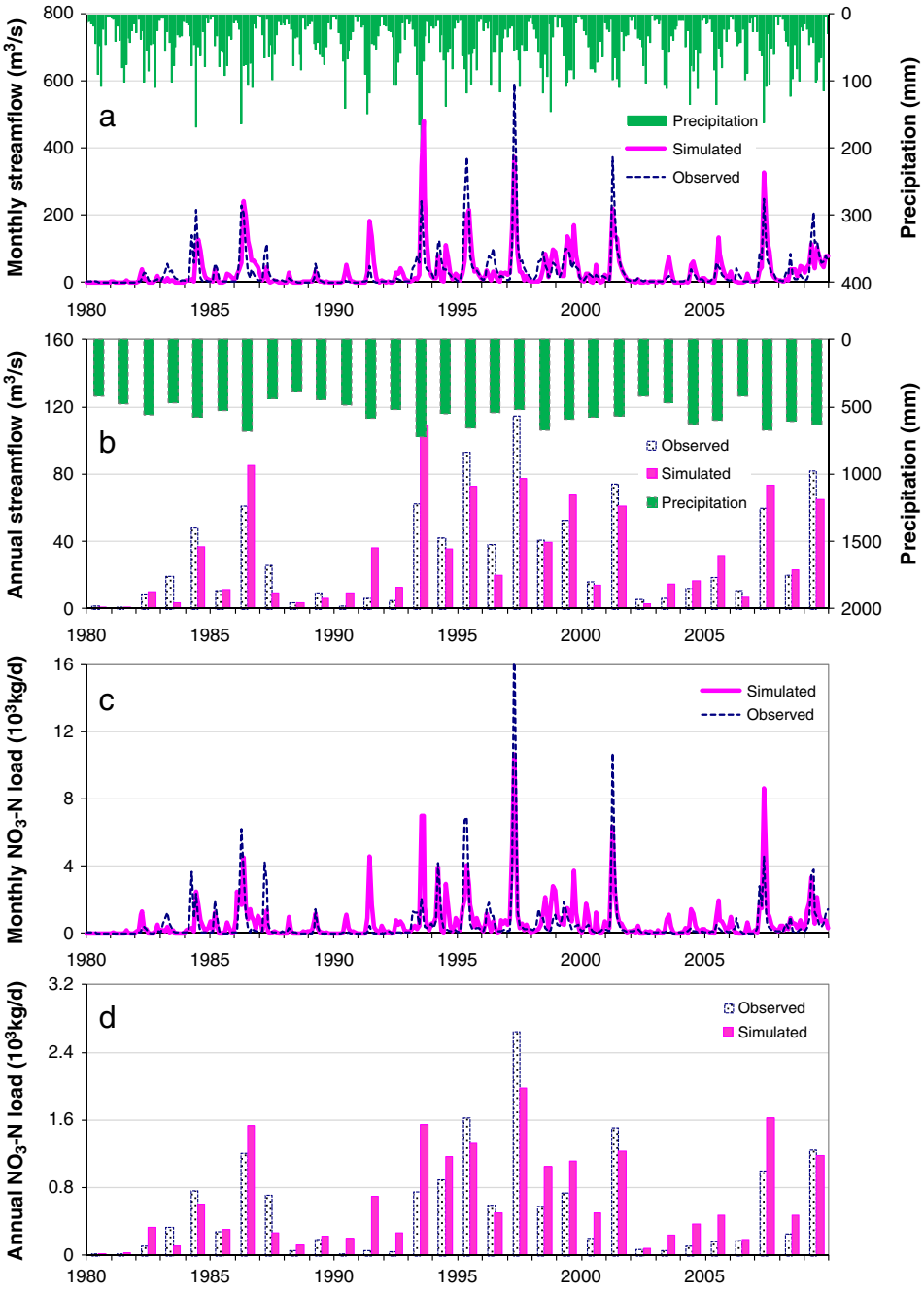

Fig. 2. Monthly and annual time series comparison of simulated versus observed streamflow (a and b) and NO_3–N (c and d) at the basin outlet (near Scotland, South Dakota) during the 30-year simulation (1980–2009) period.

gas emission scenario (NOAA/ESRL, 2010). Reduced ET will lead to a 26% increase in soil water content and a 49% increase in water yield, resulting in a 67% increase in groundwater recharge and a 40% increase in NO_3–N load. Damper soil can raise the water yield by generating more surface runoff, subsurface lateral flow, and seepage from soil to shallow aquifer, eventually contributing to the streamflow with NO_3–N transport.

3.2.2. Precipitation

Scenarios 3 through 6 reflect precipitation changes of +10%, +20%, −10% and −20% while holding the baseline CO_2 concentration (361 ppm) and air temperature unchanged. As shown in Fig. 3e–h and Table 4, increases or decreases in precipitation could lead directly to corresponding directional changes in water yield, soil water content, groundwater recharge, and NO^3–N load. For example, annual average water yield changes of 59%, 133%, −42%, and −69% corresponded with changes implemented for annual precipitation (Table 4). For water yield, however, substantial increases or decreases of precipitation during the wet season (Fig. 3e), especially from May to August, highlight concerns about risks to flood and drought in this basin. Fig. 3f indicates a nearly linear change in monthly soil water content in response to changes in precipitation, and annual average soil water content could increase as much as 33% or decrease as much as 41% under precipitation scenarios of 20% increase or decrease, respectively (Table 4). The absolute response of groundwater recharge is marked during the wet season; ±10% change in precipitation could cause nearly +70% or −50% changes in annual groundwater recharge (Fig. 3g). Similarly,

Table 3
Evaluation of model performance in streamflow and NO_3–N simulation at the basin outlet (near Scotland, South Dakota) during ten-year calibration (1991–2000), nine-year validation (2001–2009), and 30-year baseline (1980–2009) periods.

Period		Time scale	Mean		PB (%)	NSE	R^2
			Observed	Simulated			
Streamflow (m^3/s)	Calibration	Monthly	46.9	38.2	−18.4	0.55	0.56
		Annual				0.75	0.84
	Validation	Monthly	32.2	29.8	−7.4	0.67	0.67
		Annual				0.79	0.81
	Baseline	Monthly	32.0	32.2	0.8	0.45	0.51
		Annual				0.72	0.74
NO_3–N (kg/d)	Calibration	Monthly	830.6	849.4	2.3	0.60	0.61
		Annual				0.80	0.85
	Validation	Monthly	522.7	621.2	18.9	0.67	0.68
		Annual				0.77	0.80
	Baseline	Monthly	579.9	700.05	20.8	0.50	0.51
		Annual				0.70	0.74

a change of nearly +60% or −50% for NO_3–N load could result from ±10% change in precipitation (Fig. 3h and Table 4). Interestingly, soil water content is much less responsive to increased precipitation than is water yield Fig. 3e,f, which can be caused by the limited water-holding capacity of the soil. This emphasizes the importance of flood mitigation under a scenario of increased precipitation.

3.2.3. Air temperature

Scenarios 7 through 9 represent increases of 1 °C, 2 °C, and 4 °C for average air temperature while holding other climate elements constant (Table 2). Soil water content is little affected by a unit temperature rise of 1 °C, but is more sensitive to larger temperature rises (Fig. 3j). Higher temperatures will result in significant decreases in soil water content owing to increased ET (Fig. 3i–l). The drier soil then could cause reduction in water yield, groundwater recharge, and NO^3–N load because it affects the surface runoff, subsurface lateral flow, and baseflow, as stated previously. A small rise in the NO^3–N load in December and January can be attributed to the increased surface runoff resulting from increased snow melt in winter (Fig. 3l). Water yield and groundwater recharge reductions caused by rising temperatures are more substantial in the wet season (Fig. 3i,k), especially from May to August when plant growth responses are more significant.

Annual average soil water content is projected to decline by 5% to 49% when increases in the air temperature range from 1 °C to 4 °C

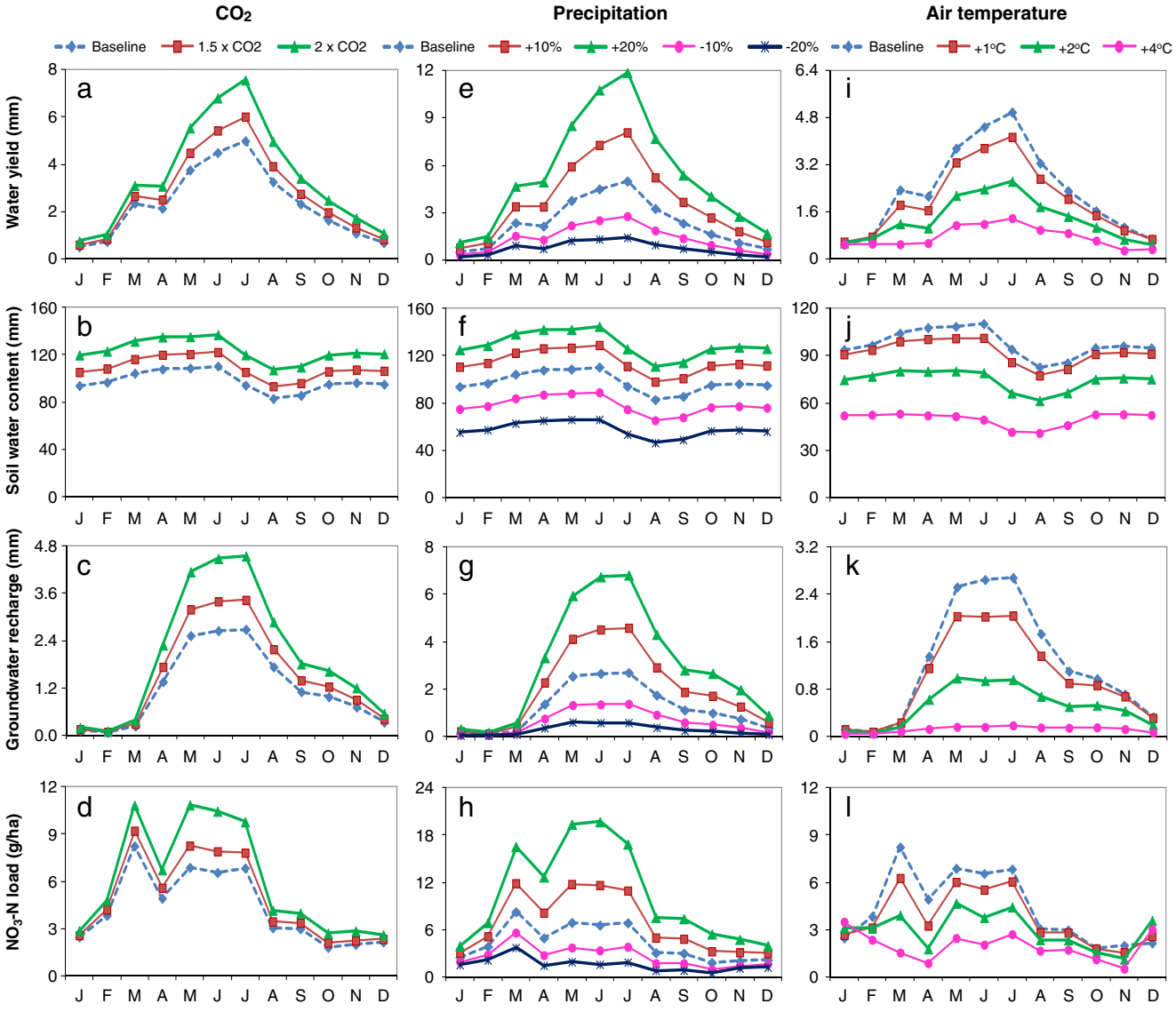

Fig. 3. Comparison of simulated monthly water yield, soil water content, groundwater recharge, and NO_3–N load under different CO_2 concentrations (a–d), precipitation change scenarios (e–h), and air temperature increase scenarios (i–l).

Table 4
Predicted relative changes (percent of baseline levels) in annual average hydrological components with climate-sensitivity scenarios and GCM projection scenarios.

Terms	Ref[a]	Climate sensitivity[b]									GCM[c]		
		CO_2		Precipitation (%)				Air temperature (°C)			B1	A1B	A2
		×1.5	×2	+10	+20	−10	−20	+1	+2	+4			
		Percent change											
WY	28	19	49	59	133	−42	−69	−14	−42	−68	−61	−68	−70
ET	533	−1	−3	7	13	−8	−16	1	3	5	−5	−4	−4
SW	98	12	26	18	33	−20	−41	−5	−24	−49	−37	−45	−48
GR	14	27	67	69	152	−49	−78	−19	−58	−91	−77	−87	−89
NO_3–N	0.05	14	40	58	142	−40	−64	−14	−31	−55	−49	−54	−55

[a] Ref means hydrological components with reference scenario.
[b] Climate sensitivity means the SWAT simulations with climate-sensitivity scenarios.
[c] GCM refers to the SWAT simulations with the averaged GCM-ensemble under the A1B greenhouse gas emission scenario; WY is water yield (mm/yr); ET is evapotranspiration (mm/yr); SW is soil water content (mm); GR is groundwater recharge (mm/yr); NO_3–N is nitrate nitrogen load (kg/ha). Positive and negative signs refer to increases and decreases, respectively.

(Table 4). Similarly, water yield may decrease by 14% to 68%, groundwater recharge may decrease 19% to 91%, and NO_3–N load may decrease by 14% to 55% under the same changes in air temperature. These results indicate global warming may lead to serious water shortages in this basin.

3.3. Projected climate-change effects

We applied the downscaled, multi-model ensemble GCM outputs with the projected CO_2 concentrations (see Section 2.5) as climate inputs for the modified SWAT model (Wu et al., 2012) to investigate hydrological effects of potential future climates for the mid-21st century. Basin average monthly precipitation and air temperatures for baseline conditions (1980–2009) and future projections (2040–2069) under three greenhouse gas emission scenarios are shown in Fig. 4. The comparison indicates a decrease of 8.5% to 9.0% in precipitation and increase of 1.9 °C to 3.1 °C among the three emission scenarios. Multiyear (2040–2069) average monthly results (water yield, soil water content, groundwater recharge, and NO_3–N) simulated by SWAT for the whole basin are presented in Fig. 5, and the annual average percent changes relative to the reference scenario are listed in Table 4. Under scenarios B1, A1B, and A2, annual water yield in this basin will decrease dramatically (about 61% to 70%) (Fig. 5a and Table 4), principally because of the projected decreases

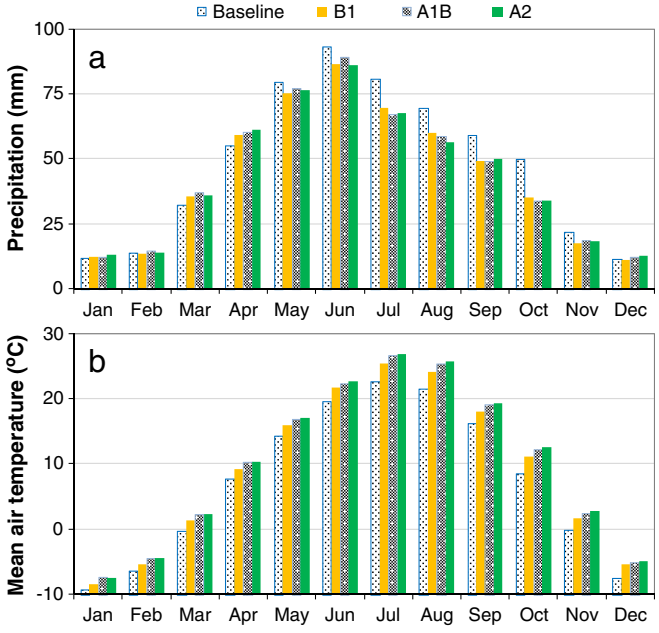

Fig. 4. Basin average monthly precipitation (a) and air temperature (b) under the baseline conditions (1980–2009) and projections (2040–2069) averaged across output from six GCMs under three greenhouse gas emission scenarios (B1, A1B, and A2).

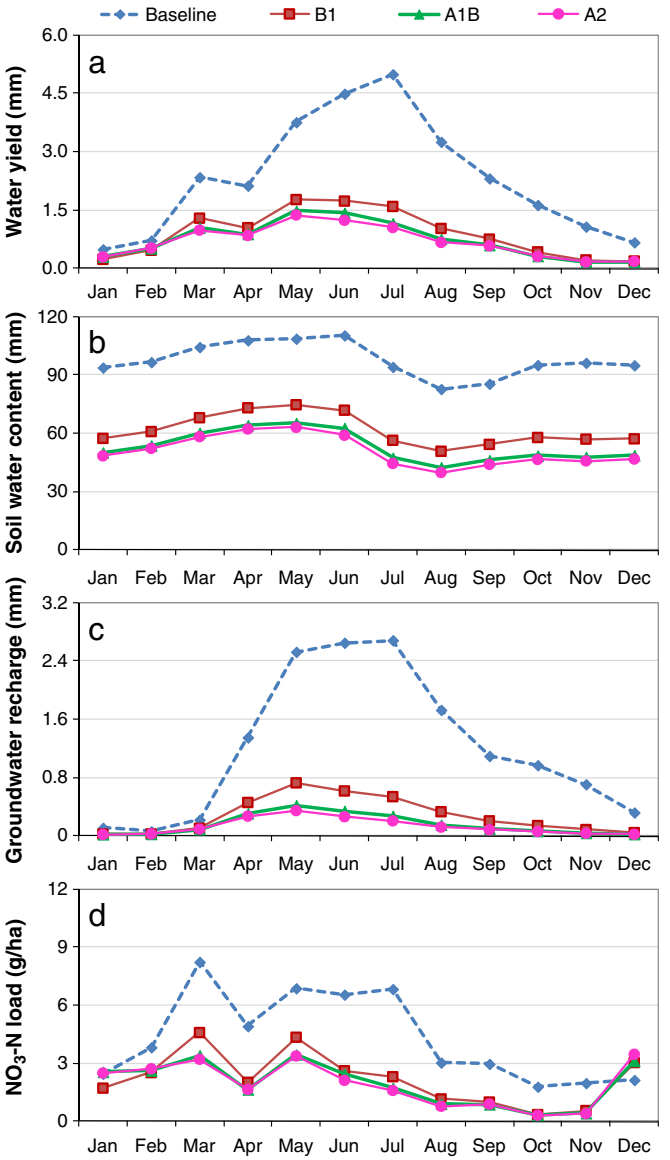

Fig. 5. Comparison of simulated water yield (a), soil water content (b), groundwater recharge (c), and NO_3–N load (d) under emission scenarios B1, A1B, and A2.

in precipitation and increases in air temperature. Annual soil water content and groundwater recharge could be reduced by about 37% to 48% and 77% to 89% (Fig. 5b,c, and Table 4), respectively, by the mid-21st century. The substantial decrease in groundwater recharge could directly reduce the aquifer storage. NO_3–N load was projected to decline 49% to 55% (Fig. 5d and Table 4); however, NO_3–N concentration in stream water would increase 55% to 70% as the amount of water in the river channel decreased.

We also compared spatial distributions (at the HRU level) of the four hydrological variables (water yield, soil water content, groundwater recharge, and NO_3–N load) under baseline conditions (see Fig. 6a,c,e,g) and projected climate conditions (see Fig. 6b,d,f,h), and present outcomes from the A1B scenario here as an example. Results show that the relatively higher annual water yield in the mid-basin area under baseline conditions may decline to a level comparable with other parts of the basin under the projected climate (Fig. 6a,b). This could reduce the spatial variability of the annual water yield by 23% in terms of the standard deviation (a shift from 47.8 to 36.4 mm). The projected climate also could reduce the annual soil water content substantially, with an average decrease of 38% over the entire basin and a corresponding decrease of 32% in the standard deviation of the spatial variability (Fig. 6c,d). Moreover, areas in the upper and lower basin may experience severe drought with this climate scenario (Fig. 6d). The reduced soil water content could lead to a significant decrease in groundwater recharge (Fig. 6e,f), with an associated reduction of 31% in the standard deviation of the spatial variability in recharge across the basin. Basin average NO^3–N load would decrease by about 31% due to the reduction in water yield, with substantial decrease occurring on higher nitrogen load areas (mid-basin) (Fig. 6g,h).

4. Discussion

4.1. Model performance

We identified substantial differences between observed and modeled peak flows (e.g., 1991 and 1993), maybe because the limited number of rainfall gages are not sufficient to reflect spatial patterns of rainfall over such a large basin for certain years. We noted an underestimation for 1997, possibly attributed to the intensified rainfall (at a smaller time scale like hours) that year causing high streamflows despite an overall moderate amount of annual precipitation (Fig. 2b) (see also (Zhou et al., 2011)). Although the above factors contributed to relatively low model efficiency, the monthly streamflow simulations can be evaluated as “satisfactory” (NSE > 0.5 and |PB| ≤ 25%) and “good” (NSE > 0.65 and |PB| ≤ 15%)

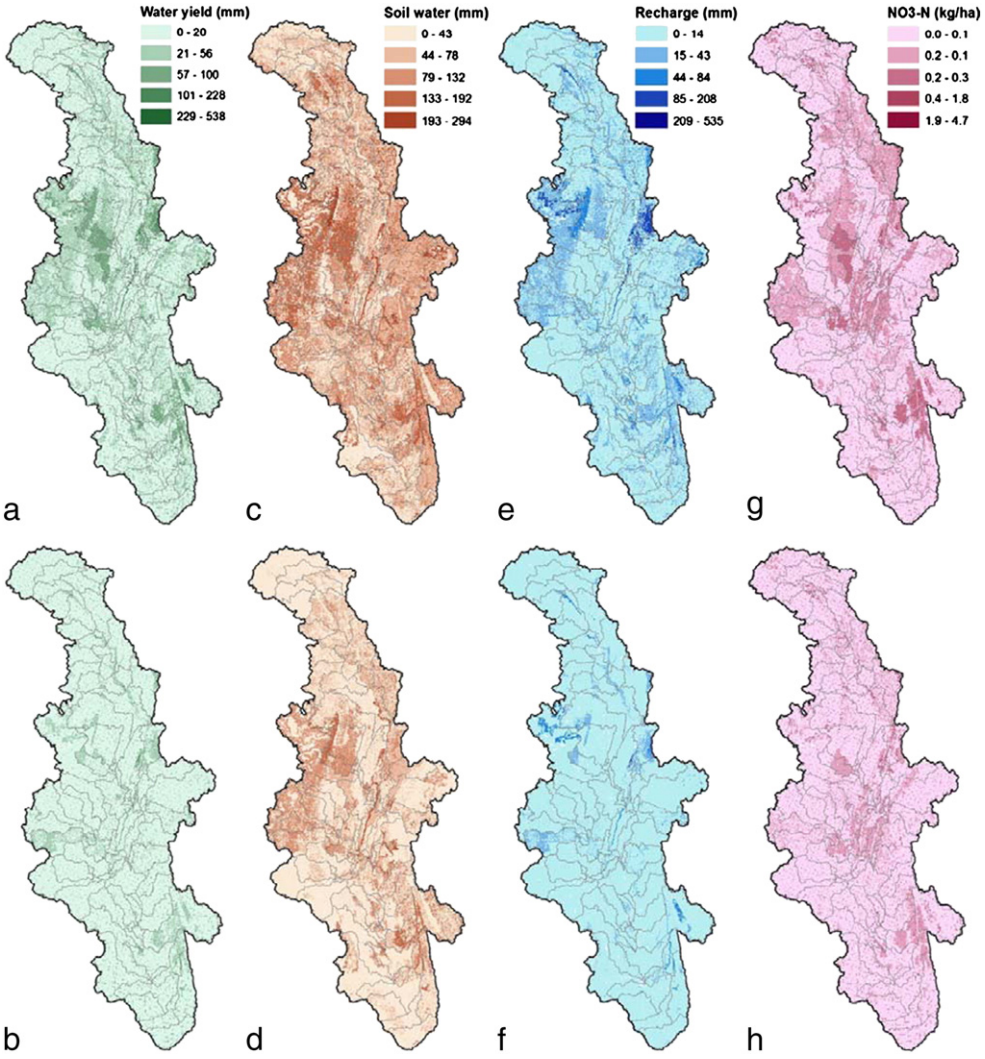

Fig. 6. Comparison of the spatial distributions of water yield (a versus b), soil water content (c versus d), groundwater recharge (e versus f), and NO_3–N load (g versus h) under baseline conditions (upper panels) and the climate projected with the A1B scenario (lower panels). These four hydrological variables represent average annual results for the 30-year baseline period (1980–2009) and projection period (2040–2069).

for calibration and validation periods, respectively, based on the performance ratings of Moriasi et al. (2007), which assume typical uncertainty in observations. Because our climate-change study focuses on long-term (30 years) impacts rather than impacts from single events or a few years, the model performance can be deemed acceptable for this study, especially given our use of multiyear average simulation results.

4.2. Climate change impacts

As stated previously (see Section 2.6), an explicit assumption with the downscaling technique we used is that future geospatial patterns of climate will be the same as those of the past. There is no way to know how such patterns will change in the future within the JRB, but information from the past provides at least one plausible (documented) way to distribute geospatial patterns. The accuracy of the GCM projections is unknown, although the averaged results indicate a decrease in precipitation and an increase in air temperature. If the annual precipitation in the JRB decreases as expected from the GCM multi-model ensemble, even under the A1B scenario the decline in groundwater recharge (see Table 4) would be a critical concern for stream water availability especially in the dry season when baseflow is the dominant contributing source. This can be revealed by the low level of dry season water yield as shown in Fig. 5a. Although a related substantial decrease in NO_3–N load appears to be a benefit, the increase in NO_3–N concentration in stream water as water yield decreased would result in degraded water quality. Overall, the projected decreases in soil water content, groundwater recharge, and water yield, and the increase in NO_3–N concentration would pose potential threats for crop production and water quantity and quality in this basin.

5. Implications

The climate sensitivity study helped quantify responses of the JRB hydrology and water quality to rising levels of atmospheric CO_2 concentration and potential changes in precipitation and air temperature. Our analysis of hydrological effects under a projected climate trajectory demonstrated how and to what magnitude the JRB hydrology and water quality could be altered in the future, although we recognize that uncertainties with GCMs likely increase with the length of the projection period. Therefore, the climate-sensitivity analysis can be indispensable. Overall, both climate-sensitivity scenarios and GCM projections are useful for informing water resource managers and other decision makers about precautions that may be needed to mitigate potential watershed problems related to floods and drought and associated concerns with water supply, water quality, food production, and risks to human health and property.

Comparison of the JRB hydrological response with those in the adjacent Upper Mississippi River Basin (see Fig. 1) from our previous study (Wu et al., 2012) suggests the hydrological system in this semiarid basin is relatively more sensitive to climate change. Therefore, this region specific study may alert that watershed managers for drier basins should take more precautions to cope with the potential water issues due to climate change such as the relatively higher variability of water yield which may cause extreme events like flooding and drought.

6. Conclusions

We applied a modified SWAT model that incorporates plant responses (stomatal conductance reduction and leaf area increase) to elevated CO_2 concentrations, to investigate hydrological effects of rising CO_2 concentrations and climate change in the JRB. Our analysis of the sensitivity of hydrological variables to shifts in climate revealed the hydrological system in this semiarid basin is highly responsive. For example, water yield, soil water content, groundwater recharge, and NO^3–N load could increase about 49%, 26%, 67%, and 40%, respectively, under a doubling of CO_2 concentration. Nearly linear responses in levels of water yield (−69% to 133%) and soil water content (−41% to 33%) were predicted when precipitation changes ranged from −20% to +20% relative to 1980–2009 baseline levels. All four hydrological components could decrease substantially with rises in air temperature.

Climate trajectories for three greenhouse gas emission scenarios (B1, A1B, and A2) for 2040 through 2069 suggest decreases in precipitation ranging from 8.5 to 9.0% and increases in air temperature ranging from 1.9 to 3.1 °C. Under these climate conditions, hydrological components could be altered considerably. Soil water content, water yield, and groundwater recharge could decrease over 61%, 37%, and 77%, respectively, and changes in the spatial distribution of these characteristics would have differential impacts across the basin. Although the NO^3–N load may decrease more than 49%, the projected increase of about 55% in NO^3–N concentration in stream water would be of concern for water quality and the aquatic environment.

No one knows with certainty how climate change will play out over the coming decades, given the myriad interactions in the Earth's environment, but modeling assessments such as we have undertaken offer advanced insights into potential ranges for consequences. Our combined analyses of sensitivity of hydrological components to climate change and the effects of different scenarios of future climate on the direction, magnitude, and spatial distribution of hydrological responses provide needed input for consideration towards watershed management and policies.

Acknowledgments

This study was funded by the NASA Land Cover and Land-Use Change Program (Grant NNH07ZDA001N) and the U.S. Geological Survey Geographic Analysis and Monitoring Program. The majority of this work was performed under USGS contract G08PC91508. Any use of trade, firm, or product names is for descriptive purposes only and does not imply endorsement by the U.S. Government. We thank Lauren Hay, Steve Markstrom, and Christian Ward-Garrison for modifying and sharing their GCM output downscaler. We thank Ramesh Singh and Elisabeth Brouwers for comments on the early version of this paper. We also thank the two anonymous reviewers for their invaluable and constructive comments and suggestions for improving the paper quality.

Appendix A

We adopted widely accepted criteria to assess the SWAT model performance against observations.

(I) The *Percentage Bias (PB)* measures the average difference between measurements and model simulations. The optimal value of PB is 0.0, with low-magnitude values indicating accurate model simulation and positive or negative values indicating over-prediction or under-prediction bias, respectively:

$$PB = \frac{1}{n}\sum_{i=1}^{n}\left(\frac{Y_{i,\mathrm{sim}} - Y_{i,\mathrm{obs}}}{Y_{i,\mathrm{obs}}} \times 100\right)$$

(II) The *Nash–Sutcliffe Efficiency (NSE)* (Nash and Sutcliffe, 1970) measures the goodness of fit and approaches unity if the simulation is satisfactorily representing the observations. The NSE describes the explained variance for the observed values over time that is accounted for by the model (Green and van Griensven, 2008). If the

efficiency becomes negative, model predictions are worse than a prediction performed using the average of all observations:

$$NSE = 1 - \frac{\sum_{i=1}^{n}\left(Y_{i,\mathrm{sim}} - Y_{i,\mathrm{obs}}\right)^2}{\sum_{i=1}^{n}\left(Y_{i,\mathrm{obs}} - \bar{Y}_{\mathrm{obs}}\right)^2}$$

(III) The R^2 evaluates how accurately the model tracks the variation of the observed values. It can reveal the strength and direction of a linear relation between the simulation and observation. The difference between the NSE and the R^2 is that only the NSE can interpret model performance in replicating individually observed values (Green and van Griensven, 2008):

$$R^2 = \frac{\left(\sum_{i=1}^{n}\left(Y_{i,\mathrm{obs}} - \bar{Y}_{\mathrm{obs}}\right)\left(Y_{i,\mathrm{sim}} - \bar{Y}_{\mathrm{sim}}\right)\right)^2}{\sum_{i=1}^{n}\left(Y_{i,\mathrm{obs}} - \bar{Y}_{\mathrm{obs}}\right)^2 \sum_{i=1}^{n}\left(Y_{i,\mathrm{sim}} - \bar{Y}_{\mathrm{sim}}\right)^2}$$

where n is number of observation/simulation data for comparisons; $Y_{i,\mathrm{obs}}$ and $Y_{i,\mathrm{sim}}$ are observed and simulated data, respectively, on each time step i (e.g., day or month); and $\bar{Y}_{\mathrm{obs}}$ and $\bar{Y}_{\mathrm{sim}}$ are mean values for observation and simulation during examination period.

References

Arabi M, Frankenberger JR, Enge BA, Arnold JG. Representation of agricultural conservation practices with SWAT. Hydrol Process 2008;22:3042–55.

Arnell NW, Liv C. Hydrology and water resources. In: McCarthy JJ, Canziani OF, Leary NA, Dokken DJ, White KS, editors. Climate Change 2001: impacts, adaptation and vulnerability. Cambridge, UK: Cambridge University Press; 2001.

Arnold JG, Srinivasan R, Muttiah RS, Williams JR. Large area hydrologic modeling and assessment—part 1: model development. J Am Water Resour Assoc 1998;34: 73–89.

Bates B, Kundzewicz ZW, Wu S, Palutikof J. Climate change and water. Technical Paper VI of the Intergovernmental Panel on Climate Change. Geneva: IPCC Secretariat; 2008. p. 210.

Betts RA, Cox PM, Lee SE, Woodward FI. Contrasting physiological and structural vegetation feedbacks in climate change simulations. Nature 1997;387:796–9.

Betts RA, Boucher O, Collins M, Cox PM, Falloon PD, Gedney N, et al. Projected increase in continental runoff due to plant responses to increasing carbon dioxide. Nature 2007;448:1037–42.

Beven KJ. Rainfall-runoff modelling. Chichester: John Wiley & Sons; 2001.

Chaplot V. Water and soil resources response to rising levels of atmospheric CO2 concentration and to changes in precipitation and air temperature. J Hydrol 2007;337:159–71.

Craig M. A history of the cropland data layer at NASS. http://www.nass.usda.gov/research/Cropland/CDL_Hisotry_MEC.pdf2010. accessed 09 December, 2011.

Duan QY, Sorooshian S, Gupta V. Effective and efficient global optimization for conceptual rainfall-runoff models. Water Resour Res 1992;28:1015–31.

Eckhardt K, Ulbrich U. Potential impacts of climate change on groundwater recharge and streamflow in a central European low mountain range. J Hydrol 2003;284: 244–52.

Ficklin DL, Luo YZ, Luedeling E, Zhang MH. Climate change sensitivity assessment of a highly agricultural watershed using SWAT. J Hydrol 2009;374:16–29.

Ficklin DL, Luo YZ, Luedeling E, Gatzke SE, Zhang MH. Sensitivity of agricultural runoff loads to rising levels of CO2 and climate change in the San Joaquin Valley watershed of California. Environ Pollut 2010;158:223–34.

Field CB, Jackson RB, Mooney HA. Stomatal responses to increased CO2—implications from the plant to the global -scale. Plant Cell Environ 1995;18:1214–25.

Fontaine TA, Klassen JF, Cruickshank TS, Hotchkiss RH. Hydrological response to climate change in the Black Hills of South Dakota, USA. Hydrol Sci J-J Sci Hydrologiques 2001;46:27–40.

Fowler HJ, Blenkinsop S, Tebaldi C. Linking climate change modelling to impacts studies: recent advances in downscaling techniques for hydrological modelling. Int J Climatol 2007;27:1547–78.

Gedney N, Cox PM, Betts RA, Boucher O, Huntingford C, Stott PA. Detection of a direct carbon dioxide effect in continental river runoff records. Nature 2006;439:835–8.

Gleckler PJ, Taylor KE, Doutriaux C. Performance metrics for climate models. J Geophys Res Atmos 2008:113.

Green CH, van Griensven A. Autocalibration in hydrologic modeling: using SWAT2005 in small-scale watersheds. Environ Model Software 2008;23:422–34.

Hay LE, Markstrom SL, Ward_Garrison C. Watershed-scale response to climate change through the twenty-first century for selected basins across the United States. Earth Interact 2011;15:1-37.

Homer C, Dewitz J, Fry J, Coan M, Hossain N, Larson C, et al. Completion of the 2001 National Land Cover Database for the conterminous United States. Photogramm Eng Remote Sens 2007;73:337–41.

Houghton JT, Ding Y, Griggs DJ, Noguer M, Linden PJvd, Dai X. Climate Change 2001: The Scientific Basis. Contribution of Working Group I to the Third Assessment Report of the Intergovernmental Panel on Climate Change. Cambridge, United Kingdom and New York, NY, USA: Cambridge University Press; 2001.

IPCC. Special Report on Emissions Scenarios. http://www.grida.no/publications/other/ipcc_sr/?src=/climate/ipcc/emission2000. accessed 09 December, 2011.

IPCC. Climate Change 2001: IPCC Third Assessment Report. http://www.ipcc-data.org/ddc_co2.html2001. accessed 1 March, 2012.

IPCC. GCM Experiment Data (AR4); 2006.

Jackson RB, Carpenter SR, Dahm CN, McKnight DM, Naiman RJ, Postel SL, et al. Water in a changing world. Ecol Appl 2001;11:1027–45.

Jha M, Arnold JG, Gassman PW, Giorgi F, Gu RR. Climate change sensitivity assessment on Upper Mississippi River Basin streamflows using SWAT. J Am Water Resour Assoc 2006;42:997-1015.

Jha MK, Schilling KE, Gassman PW, Wolter CF. Targeting land-use change for nitrate-nitrogen load reductions in an agricultural watershed. J Soil Water Conserv 2010;65:342–52.

Kergoat L, Lafont S, Douville H, Berthelot B, Dedieu G, Planton S. Impact of doubled CO2 on global-scale leaf area index and evapotranspiration: conflicting stomatal conductance and LAI responses. J Geophys Res Atmos 2002:107.

Koster RD, Dirmeyer PA, Guo ZC, Bonan G, Chan E, Cox P, et al. Regions of strong coupling between soil moisture and precipitation. Science 2004;305:1138–40.

Labat D, Godderis Y, Probst JL, Guyot JL. Evidence for global runoff increase related to climate warming. Adv Water Res 2004;27:631–42.

Labat D, Godderis Y, Probst JL, Guyot JL. Reply to comment of Legates et al. Adv Water Res 2005;28:1316–9.

Lambert SJ, Boer GJ. CMIP1 evaluation and intercomparison of coupled climate models. Clim Dyn 2001;17:83-106.

Legates DR, Lins HF, McCabe GJ. Comments on "Evidence for global runoff increase related to climate warming" by Labat et al. Adv Water Res 2005;28:1310–5.

Leipprand A, Gerten D. Global effects of doubled atmospheric CO2 content on evapotranspiration, soil moisture and runoff under potential natural vegetation. Hydrol Sci J-J Sci Hydrologiques 2006;51:171–85.

Medlyn BE, Barton CVM, Broadmeadow MSJ, Ceulemans R, De Angelis P, Forstreuter M, et al. Stomatal conductance of forest species after long-term exposure to elevated CO2 concentration: a synthesis. New Phytol 2001;149:247–64.

Moriasi DN, Arnold JG, Van Liew MW, Bingner RL, Harmel RD, Veith TL. Model evaluation guidelines for systematic quantification of accuracy in watershed simulations. Trans ASABE 2007;50:885–900.

Morison JIL. Intercellular CO2 concentration and stomatal response to CO2. Stanford, USA: Stanford University Press; 1987.

Morison JIL, Gifford RM. Stomatal sensitivity to carbon dioxide and humidity. Plant Physiol 1983;71:789–96.

Muleta MK, Nicklow JW. Sensitivity and uncertainty analysis coupled with automatic calibration for a distributed watershed model. J Hydrol 2005;306:127–45.

Nash JE, Sutcliffe JV. River flow forecasting through conceptual models. Part I a discussion of principles. J Hydrol 1970;10:282–90.

Neitsch SL, Arnold JG, Kiniry JR, Williams JR, King KW. Soil and Water Assessment Tool Theoretical Documentation, Grassland, soil and research service, Temple, TX; 2005.

NOAA/ESRL. In: Pieter T, editor. NOAA ESRL DATA; 2010. www.esrl.noaa.gov/gmd/ccgg/trends/.

Pervez MS, Brown JF. Mapping irrigated lands at 250-m scale by merging MODIS data and national agricultural statistics. Remote Sens 2010;2:2388–412.

Piao SL, Yin L, Wang XH, Ciais P, Peng SS, Shen ZH. Summer soil moisture regulated by precipitation frequency in China. Environ Res Lett 2009:4.

Pierce DW, Barnett TP, Santer BD, Gleckler PJ. Selecting global climate models for regional climate change studies. Proc Natl Acad Sci U S A 2009;106:8441–6.

Pritchard SG, Rogers HH, Prior SA, Peterson CM. Elevated CO2 and plant structure: a review. Glob Change Biol 1999;5:807–37.

Santhi C, Arnold JG, Williams JR, Dugas WA, Srinivasan R, Hauck LM. Validation of the SWAT model on a large river basin with point and nonpoint sources. J Am Water Resour Assoc 2001;37:1169–88.

Saxe H, Ellsworth DS, Heath J. Tree and forest functioning in an enriched CO2 atmosphere. New Phytol 1998;139:395–436.

Schaake JC. Water resources. In: Waggoner PE, editor. Water resources. New York: John Wiley; 1990. p. 177–206.

Sharpley AN, Williams JR. EPIC—erosion productivity impact calculator, 1. model documentation, U.S. Department of Agriculture, Agricultural Research Service. Tech Bull 1990;1768.

Stockle CO, Dyke PT, Williams JR, Jones CA, Rosenberg NJ. A method for estimating the direct and climatic effects of rising atmospheric carbon dioxide on growth and yield of crops. 2. Sensitivity analysis at 3 sites in the Midwestern USA. Agr Syst 1992a;38:239–56.

Stockle CO, Williams JR, Rosenberg NJ, Jones CA. A method for estimating the direct and climatic effects of rising atmospheric carbon dioxide on growth and yield of crops. 1. Modification of the EPIC model for climate change analysis. Agr Syst 1992b;38: 225–38.

Stone MC, Hotchkiss RH, Hubbard CM, Fontaine TA, Mearns LO, Arnold JG. Impacts of climate change on Missouri River Basin water yield. J Am Water Resour Assoc 2001;37:1119–29.

Tabor K, Williams JW. Globally downscaled climate projections for assessing the conservation impacts of climate change. Ecol Appl 2010;20:554–65.

Tebaldi C, Knutti R. The use of the multi-model ensemble in probabilistic climate projections. Philos Trans R Soc A Math Phys Eng Sci 2007;365:2053–75.
Thomas MA, Engel BA, Chaubey I. Water quality impacts of corn production to meet biofuel demands. J Environ Eng-Asce 2009;135:1123–35.
Tolson BA, Shoemaker CA. Cannonsville Reservoir Watershed SWAT2000 model development, calibration and validation. J Hydrol 2007;337:68–86.
USGS. Moderate Resolution Imaging Spectroradiometer (MODIS) Irrigated Agriculture Dataset for the United States (MIrAD-US). U.S. Geological Survey Dataset. http://earlywarning.usgs.gov/USirrigation/2002. accessed 1 March, 2012.
van Griensven A, Meixner T, Grunwald S, Bishop T, Diluzio A, Srinivasan R. A global sensitivity analysis tool for the parameters of multi-variable catchment models. J Hydrol 2006;324:10–23.
Vicuna S, Maurer EP, Joyce B, Dracup JA, Purkey D. The sensitivity of California water resources to climate change scenarios. J Am Water Resour Assoc 2007;43:482–98.
Wand SJE, Midgley GF, Jones MH, Curtis PS. Responses of wild C4 and C3 grass (Poaceae) species to elevated atmospheric CO2 concentration: a meta-analytic test of current theories and perceptions. Glob Change Biol 1999;5:723–41.
Williams JR. Chapter 25. The EPIC Model. Computer Models of Watershed Hydrology. Highlands Ranch, CO: Water Resources Publications; 1995. p. 909-1000.
Wilson CO, Weng Q. Simulating the impacts of future land use and climate changes on surface water quality in the Des Plaines River watershed, Chicago Metropolitan Statistical Area, Illinois. Sci Total Environ 2011;409:4387–405.
Winchell M, Srinivasan R, Di Luzio M, Arnold JG. ArcSWAT 2.3.4 Interface For SWAT2005, Grassland, soil and research service, Temple, TX; 2009.
Wu Y, Liu S, Abdul-Aziz OI. Hydrological effects of the increased CO2 and climate change in the Upper Mississippi River Basin using a modified SWAT. Clim Change 2012;110:977-1003.
Xu ZX, Zhao FF, Li JY. Response of streamflow to climate change in the headwater catchment of the Yellow River basin. Quat Int 2009;208:62–75.
Young CA, Escobar-Arias MI, Fernandes M, Joyce B, Kiparsky M, Mount JF, et al. Modeling the hydrology of climate change in California's Sierra Nevada for subwatershed scale adaptation 1. J Am Water Resour Assoc 2009;45:1409–23.
Zhang XS, Srinivasan R, Bosch D. Calibration and uncertainty analysis of the SWAT model using genetic algorithms and bayesian model averaging. J Hydrol 2009;374:307–17.
Zhou G, Wei X, Wu Y, Liu S, Huang Y, Yan J, et al. Quantifying the hydrological responses to climate change using an intact forested small watershed in Southern China. Glob Change Biol 2011;17:3736–46.